Mechanical Simulation of Neural Electrode-Brain Tissue Interface Under Various Micromotion Conditions

Wenguang Zhang [1,*] Zhengwei Li[1] Merceron Gilles[1,2] Dongdong Wu[1]

[1]*State Key Laboratory of Mechanical System and Vibration, Shanghai Jiao Tong University, Shanghai 200240, China*
[2]*Arts et Métiers ParisTech, 75013 Paris, France*

Received 28 Jan 2013; Accepted 8 Apr 2013; doi: 10.5405/jmbe.1444

Abstract

Micromotion is one of the most important factors that influence the long-term stability of neural electrodes. In order to improve the long-term stability of brain-implanted electrodes, this study uses finite element simulation for static and transient analyses. In particular, the effects of micromotion frequency and adhesion state on the mechanical state of the electrode-brain tissue interface are investigated based on the commercial electrode A1x16-3-100-413. The results demonstrate that micromotion frequency has a great effect on the maximum von Mises (VM) stress, revealing that higher frequencies are more harmful than lower frequencies in terms of the long-term stability of the electrode. When the frequency is 20 Hz, the stress reaches its maximum value, and then increases very slightly with frequency increasing. Results also show that the degree of physical coupling between the electrode and the brain tissue has a significant influence on the interfacial mechanical state. Enhancing the adhesion between the electrode and the brain tissue can effectively decrease the stress, strain, and delamination of the microelectrode tip with respect to the adjacent neural tissue, and thus improve the working life of implanted electrodes. The cyclic hysteresis energy is highly dependent on the adhesion of the electrode-tissue interface; the energy values are highest for a low electrode-tissue physical coupling. The results indicate that it is important to minimize the micromotion of the brain tissue caused by neural electrodes. A neural electrode with a biofouling-resistant coating should thus be developed to optimize the interface to enhance the adhesion between the brain tissue and electrodes.

Keywords: Microelectrode, Finite element method (FEM), Micromotion, Modeling and simulation, Physical coupling

1. Introduction

Neural microelectrodes are generally used to connect the nervous system to external devices. Deep brain stimulation is a neurosurgical treatment that stimulates the deep brain with electrical signals. It has become a highly successful therapy that alleviates the symptoms of some treatment-resistant disorders, such as chronic pain [1], Parkinson's disease [2], tremors [3], and dystonia [4]. A neural electrode transforms the electric current from the stimulator into an ionic biological current. It has been found that the lifetimes of recording and stimulating neural prostheses are quite short. Some researchers have achieved neural recording for a period of several months [5], but this still does not meet practical requirements. It has been confirmed that the biofouling on the neural electrode surface during the application process affects the work life of the electrode.

A multi-stage response following microelectrode insertion has been reported [6,7]. The initial insertion of an electrode into the soft tissue causes trauma, such as the tearing of neurons, glia, and blood cells. The early tissue response typically lasts 2-4 weeks and includes inflammation, increased astrocyte proliferation, the presence of reactive astrocytes, and the growth of astrocytes. The severity of the early response is related to the magnitude of the insertion trauma, which correlates to the device size and geometry. The sustained reactive response, which follows the early response, is independent of the implant size and shape. The sustained response is characterized by the formation of a dense and compact fibrous tissue. The dense fibrous tissue, which is generally generated 6 weeks after insertion and composed of reactive astrocytes and reactive microglia, reduces the electro-ionic conduction between the electrode and neurons. This encapsulation progressively leads to device failure over the long term. Other possible causes for encapsulation are tethering forces from interconnects [8], poor biocompatibility of the implanted substrate material [9,10], chronic contact with the meninges [11], and, very importantly, the relative micromotion between the brain tissue and the neural electrode, which is one of the key factors. Unfortunately, the influence of micromotion is still unclear due to the complexity

* Corresponding author: Wenguang Zhang
Tel: +86-21-34204851; Fax: +86-21-34204851
E-mail: zhwg@sjtu.edu.cn; zwgsjt@yahoo.com

of the brain-electrode interface. It is very difficult to achieve accurate test results from animal experiments.

Many studies have been conducted on the influence of micromotion. Results show that micromotion has three origins [12]: (1) mechanical sources, which include the vibrations transmitted to the electrode via its attachment system with the skull, (2) behavioral sources, which comprise movements of the entire body, and (3) physiological sources, which include the cardiac rhythm and fluctuations in respiratory pressure. There are two types of brain pulsation: a high-frequency, low-amplitude pulsation synchronous with cardiac pulses and a low-frequency, high-amplitude pulsation synchronous with breathing. Surface micromotion displacements in anesthetized rats have been observed to be 2-25 μm due to pressure changes during respiration and 1-3 μm due to vascular pulsations [13]. Brain movements of 30-40 μm were observed in a head-fixed rat running on a track ball [14], which could be related to forces resulting from the acceleration of the animal's head [15].

Micromotion is generated by the superposition of various vibration sources. The amplitude and frequency are complex and uncertain, and their influence on the mechanical state is not clear, thus limiting the development of new types of electrode. Therefore, the damage mechanism of micromotion and methods for controling micromotion have received a lot of attention in neural electrode research.

The finite element method is one of the most effective methods for studying the micromotion of electrodes. A study using a three-dimensional (3D) finite element model has been carried out to quantitatively map the strain field induced by brain micromotion between a single electrode and the brain for a range of interface conditions [16]. Another study used a 3D finite element model to investigate the mechanical strain profiles induced in the tissue as a function of substrate stiffness [17]. These studies focused on the brain strain state under static load and provided a very primary and important understanding of the influence of micromotion. However, for a real implanted electrode, the amplitude and frequency of micromotion are complex and changeable, and thus static analysis does not completely reflect the real mechanical state.

Therefore, this study is directed to understand the influence of loading and micromotion frequency on the brain stress, strain, delamination state, and cyclic hysteresis energy [18-20] to improve our understanding of the influence of micromotion and propose possible solutions for micromotion control. The effects of micromotion frequency and the adhesion state (through adjustment of the friction coefficient) of the electrode-brain tissue interface on the mechanical state of the electrode-brain tissue interface are investigated by establishing a 3D finite element model based on the commercial electrode A1x16-3-100-413. Firstly, a static analysis was carried out to study the influence of the friction coefficient. Secondly, a transient analysis with a viscoelastic model was conducted to investigate the effects of micromotion frequency, the friction coefficient, and the brain mechanical state in both short and long loading periods. It is anticipated that the analysis of the strain field distribution on the interface and the loading effects on the neural electrode may provide useful information, which can be used to enhance the biocompatibility and longevity of neural sensing in the brain.

2. Materials and methods

2.1 Finite element model

A 3D finite element model of the electrode-brain tissue interface was developed in ANSYS 11.0 (ANSYS, Inc., Canonsburg, PA). In this study, it is assumed that the neural electrode is implanted in the brain. The model has two components: a single-shank electrode and cortical brain tissue. The electrode used in the simulation is based on the geometry of a common silicon-substrate single-shank electrode from NeuroNexus Company. The A1x16-3-100-413 model was chosen because of its widespread use for both chronic and acute recording. This study investigates the electrode micromotion in only one direction (aligned with the electrode height) even though brain micromotion has no preferred direction. For loading in the longitudinal direction, there are two symmetry planes. For computational efficiency, a model based on a quarter of the full geometry was built. The two symmetry planes are the XY plane and the YZ plane, with electrode displacement aligned with the Y axis. The quarter-symmetry model and the full model of the electrode are presented in Fig. 1. Assuming that the strain effects are localized near the electrode, the geometric representation of the brain is limited to the region surrounding the electrode. The boundaries of the brain model are defined to have sufficient distances from the microelectrode to avoid the disruption of the strain field. The dimensions of the brain and the electrode are presented in Table 1.

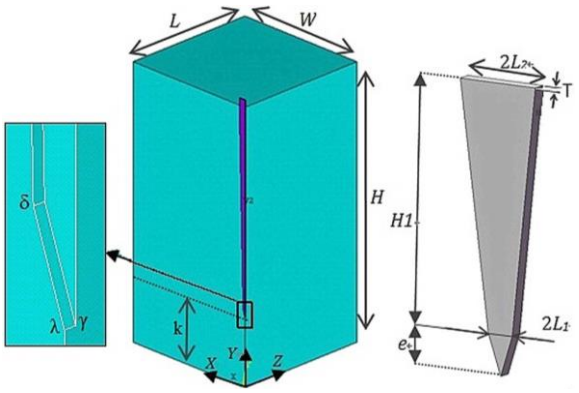

Figure 1. Schematic of simulation model. (a) Quarter-model utilized in ANSYS (blue: brain; purple: electrode). (b) Full-model of NeuroNexus electrode.

Table 1. Dimensions of quarter-model.

Name	Value (mm)	Description
L	1	Length of the brain (Z direction)
H	2	Height of the brain (Y direction)
W	1	Width of the brain (X direction)
L_1	0.016	Minimum width of the electrode (X direction)
H_1	1.5	Height of the electrode (Y direction)
L_2	0.05	Maximum width of the electrode (X direction)
T	0.0075	Thickness of the electrode (Z direction)
e	0.05	Height of the electrode tip (Y direction)
k	0.5	Height of the tip point at the beginning of the simulation

2.2 Material properties

The resulting model has 5649 elements and 8648 nodes. 3D SOLID187 elements were used for meshing. The silicon-based electrode was simulated based on a linear elastic model with a Young's modulus of 200 GPa and a Poisson's ratio of 0.278. Of note, the mechanical mismatch between the brain and silicon is so great that the deformations within the silicon electrode can be ignored during brain micromotion.

The brain tissue was considered as linear elastic and nearly incompressible for the static analysis and as viscoelastic, isotropic for the transient analysis. For the static analysis, the brain model was characterized by its Young's modulus of 15 kPa and its Poisson's ratio of 0.499 [21,22]. For the transient analysis, the brain was approximated as a viscoelastic material considering that brain properties depend on the micromotion frequency. The viscoelastic parameters used in this study are taken from a study by Nicolle et al. [23]. Nicolle et al. found that their samples exhibit linear behavior for strains under 1%, and found no anisotropy for small strains and small strain rates. Margulies and Prange found slight anisotropy during relaxation experiments [24], which has been confirmed by others to only exist for high strain rates [25,26]. The experimental shear modulus relaxation data from [23] were input into the curve fitting tool of ANSYS for viscoelastic materials. The Prony series coefficient was calculated using the curve fitting tool as the experimental input data.

2.3 Boundary conditions

The electrode and the brain tissue of the quarter-model were both subjected to symmetry boundary conditions on their XY and YZ planes. At the initial status of the simulation, the surfaces of the electrode and the brain tissue are in contact with each other. The interface between the brain and the electrode is created using ANSYS Contact Manager; the electrode is assigned as the rigid part of the model and the brain is assigned as the flexible part of the model. Various interface adhesion conditions can be simulated by varying the friction coefficient between the brain and the electrode. In this study, two kinds of adhesion condition, namely a bonded interface and a rough interface, are investigated. The former defines an interface where there is no slip between the contact surfaces, whereas the latter allows an elastic finite slip between the contact surfaces. For both adhesion conditions, the pre-simulation conditions are the electrode and the brain being in contact at a given initial position. Several values of the friction coefficient μ (from 0 to 0.5) are investigated for the rough interface, with an allowable elastic slip value of 0.005.

In reality, the electrode is attached to the skull while brain brings forward the motionless electrode. Nevertheless, brain motion is restricted within the skull, with the cerebrospinal fluid (CSF) filling the voids between the arachnoid mater and the pia mater. For modeling convenience, a reverse loading condition is applied. To simulate the micromotion, the equivalent loading mode is mimicked by applying a displacement load to the electrodes and whilst brain is blocked over its bottom surface (plane Y = 0 in Fig. 1). In this study, only longitudinal micromotion is studied since it is the most harmful amongst the six possible degrees of freedom in the brain. Both static and cyclic displacements are applied to the model to investigate the respective effects of brain-electrode adhesion conditions and the micromotion frequencies. In order to maintain consistency with the linear viscoelastic isotropic model of the brain, the micromotion amplitude is taken as 3 μm, with a frequency varying between 0 and 50 Hz. As found in [12], the micromotion has an obvious dependence on vasculature and respiratory activity, which can be represented as sinusoidal signals. In order to facilitate further utilization of the results, the micromotion $\Delta(t)$ is simplified as a perfect sinusoid applied on the top surface of the electrode in the Y direction:

$$\Delta = \alpha \sin 2\pi f t + \beta \quad (1)$$

where α is the amplitude, β is the offset of the signal, f is the frequency, and t is the time.

2.4 Simulations

Static and transient analyses were conducted for the simulations. Static analysis: Y-axis; $\Delta = 3$ μm with $f = 0$ Hz, $\alpha = 0$ μm, and $\beta = 3$ μm; linear elastic brain; bonded ($\mu = 1$) and rough (μ from 0 to 0.5) cases. Transient analysis: Y-axis; $\alpha = 1.5$ μm, $\beta = 1.5$ μm, and f varying from 0 to 50 Hz; viscoelastic brain; bonded ($\mu = 1$) and rough ($\mu = 0.2$ or 0.05) cases. Transient analyses were conducted to observe the influence of frequency on the short- term (2 loading-unloading cycles) and long-term (24 loading- unloading cycles) responses. The simulation outputs include displacements, equivalent VM strains, and VM stresses observed at the tip of the electrode (node λ, initial position: X = 0; Y = k; Z = 0), which are apt to generate stress concentration.

3. Results and discussion

3.1 Static analysis

3.1.1 VM stress and VM strain

Static analysis with a linear elastic brain model was conducted to investigate the effect of the friction coefficient. As expected, it was found that the VM stress decreases with increasing physical coupling degree. The affected zone also increases with increasing adhesion between the brain and the electrode. As shown in Fig. 2, the VM stresses and the VM strains observed for $\mu = 0$ and 0.5 are 5 and 3 times greater than those for the bonded case, respectively.

3.1.2 Delamination

The gap created by delamination is filled by various fibrous tissues, blood vessels, and scar tissue, which increases the impedance of the interface, damaging the brain tissue and degrading the electrical properties of the electrode. It is thus necessary to investigate delamination. In this model, for each case, delamination was investigated in terms of the deformation of the tissue from the electrode close to the tip.

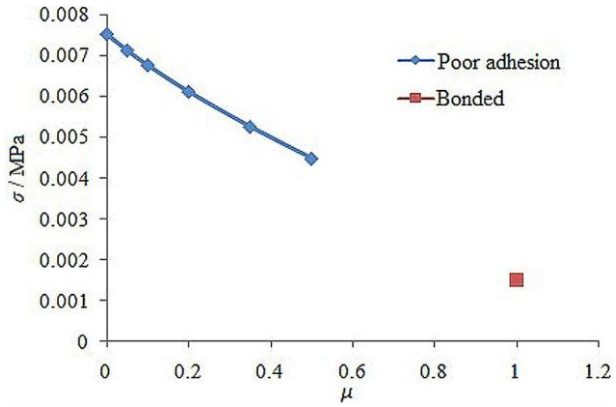

Figure 2. Influence of friction coefficient μ on maximum of VM stress.

Just like the VM stress, delamination along the Z axis decreases with increasing adhesion degree. Table 2 shows delamination values along the Z axis observed on the node near the tip of the electrode (node γ, initial position: X = 0; Y = k; Z = T/2). The simulations also reveal that delamination occurred along the X axis near the tapering sidewalls (node δ, initial position: X = L_1; Y = k + e; Z = 0). The delamination along the X axis decreases with increasing adhesion degree.

Table 2. Observed delamination over a range of friction coefficients.

friction coefficient, μ	Delamination along Z axis on node γ (μm)	Delamination along X axis on node δ (μm)
0	0.62	0.56
0.05	0.56	0.52
0.1	0.52	0.49
0.2	0.45	0.44
0.35	0.37	0.35
0.5	0.30	0.27
Bonded	None	None

3.2 Transient analysis

3.2.1 Short-term response

In this analysis, it was observed that VM stress increases with increasing frequency for all adhesion cases, whereas VM strain is independent of the electrode micromotion frequency. As shown in Fig. 3, the micromotion frequency has a greater influence on VM stress in the 0-20 Hz range than in the 20-50 Hz range.

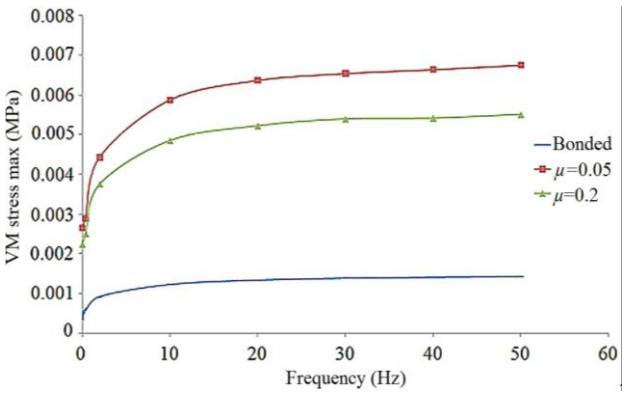

Figure 3. Influence of frequency f on VM stress.

The values for the poor adhesion case were much greater than those for the bonded case. The frequency has greater influence in the bonded case than in the poor adhesion cases: for the bonded case, the value for f = 50 Hz is 3 times greater than that for f = 0 Hz; for μ = 0.05 and 0.2, the values for f = 50 Hz are 2.5 times greater than those for f = 0 Hz.

In this study, the functional relation between stress and strain was observed in the terms of the hysteresis loop. Each hysteresis loop corresponds to the energy dissipated during the fatigue life cycle of the specimen. The value of the dissipated energy was calculated by numerically integrating of the area enclosed within the hysteresis loops. In this process, the heat dissipated energy (hysteresis heat loss) brings out cyclic softening, and as a result, shortens fatigue life. Figures 4 and 5 show the influence of friction coefficient and frequency on the cyclic hysteresis energy.

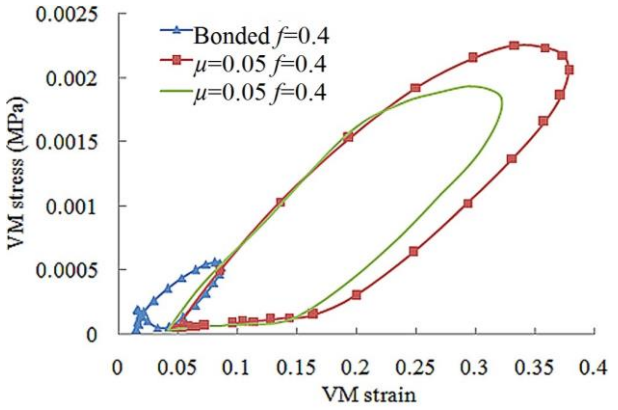

Figure 4. Influence of friction coefficient μ on hysteresis loop (f=0.4 Hz).

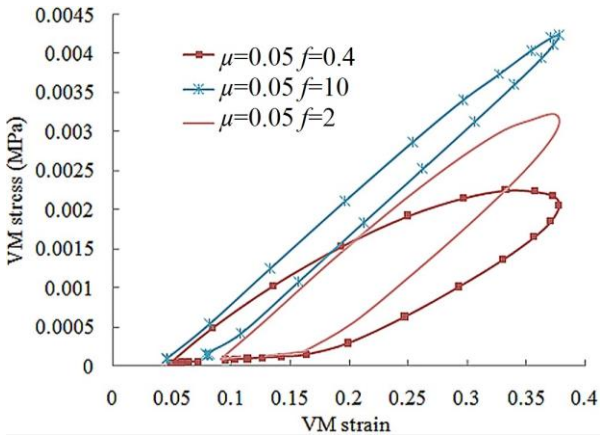

Figure 5. Influence of frequency f on hysteresis loop (μ = 0.05).

As shown in Fig. 4, the area of the loop decreases with increasing degree of physical coupling between the brain and the electrode. The shape of the loop does not change with μ in the rough case, but that for the rough case is much different from that for the bonded case. For f = 0.4 Hz, the loop area in the bonded case is only 5.5% of the whole loop area for μ = 0.05, and the loop area for μ = 0.2 is 72.7% of that for μ = 0.05. These results are consistent with the influence of the friction coefficient discussed above: when the degree of physical coupling between the brain and the electrode is increased, the values of stress and strain decrease and therefore the hysteresis loop area decreases.

As shown in Fig. 5, with a constant friction coefficient, the shape of the loop changes with frequency. The single-loop area increases with decreasing frequency. For μ = 0.05, the single-loop area for f = 10 Hz is 43.7% of that for f = 0.4 Hz, whereas that for f = 2 Hz is 75% of that for f = 0.4 Hz. The change in the shape of the loop can explain these results: the frequency has no effect on VM strain but has an effect on VM stress. Within a given period of time, the total hysteresis energy at high frequency is larger than that at low frequency, revealing that the lifetime is shortened under high-frequency conditions.

3.2.2 Long-term response

In the transient analysis, 24 loading-unloading cycles were applied to study the long-term effects of cyclic sinusoid loads.

For the rough interface, under the conditions of μ = 0.05 and 0.2, after 24 loading-unloading cycles, the maximum value of VM stress decreases while the minimum value remains constant; the minimum value of VM strain increases while the maximum value remains constant. As shown in Fig. 6, for the rough interface, the evolution trends of VM strain and VM stress values are the same under the conditions of μ = 0.05 and 0.2 while greater stress values were obtained for μ = 0.05. In the short-term response, it was observed that the frequency has no effect on the maximum values of VM strain but has an effect on the maximum values of VM stress. These observations are also valid for the long-term response.

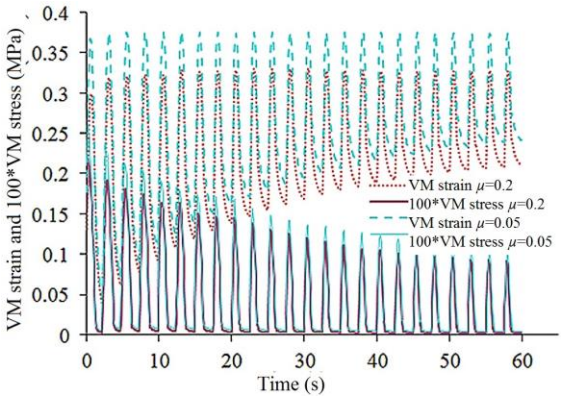

Figure 6. Evolution of VM stress and VM strain over the long term (f = 0.4 Hz).

When keeping the friction coefficient constant while varying the frequency, the frequency has no influence on the maximum values of VM strain but has an influence on the minimum values of VM strain. The minimum values of strain increase faster for lower frequencies than for higher frequencies.

The micromotion frequency has an effect on the maximum values of VM stress whereas it has no influence on the minimum values of VM stress. The maximum VM stress value is larger for higher frequencies than for low frequencies, consistent with the results of Fig. 3.

The delamination on nodes δ and γ was investigated in the long-term transient analysis. The delamination states of nodes δ and γ are the same as those obtained in the static analysis, but with different maximum values. Therefore, the X delamination on node δ and the Z delamination on node γ are taken as examples. The delamination varies sinusoidally responded to the applied displacement load. As shown in Fig. 7, the minimum delamination value increases while the maximum value remains constant with increasing number of loading-unloading cycles. The influence of μ and f on delamination is exactly the same as that on the VM strain on node λ: μ has an effect on the maximum values but not on the evolution rate of the minimum value; f has no influence on the maximum values but has an effect on the increasing rate of minimum values. When μ is decreased, both the minimum and maximum values of delamination increase; when f is increased, the maximum value remains constant, and the increasing rate of minimum values decreases.

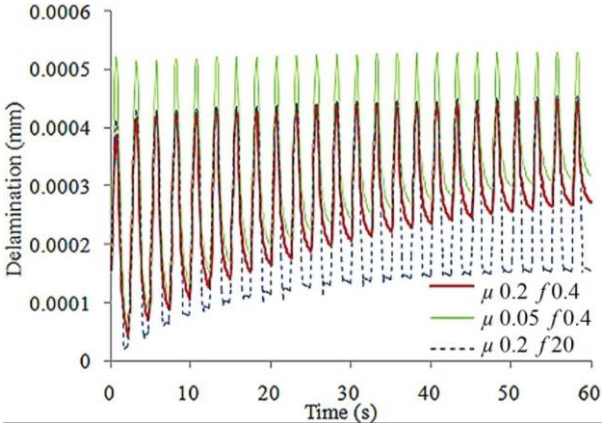

Figure 7. Effects of friction coefficient μ and frequency f on long-term delamination in Z direction.

As time increases, the size of the loading-unloading loop decreases and the minimum values of the VM strain increasing while the maximum values remain constant. For the VM stress, the maximum values decrease while the minimum values remain constant. As shown in Fig. 8, the size of each loading-unloading loop decreases with time; for f = 0.4 Hz andμ = 0.2, the area of the 24th loop is 15.7% of that of the first loop. For f = 20 Hz, the 24th loop is 22.8% of that of the first loop. The shape of the loop does not change over time. The total hysteresis energy at high frequency is larger than that at low frequency, revealing that the lifetime is shortened under high frequency over a given period of time.

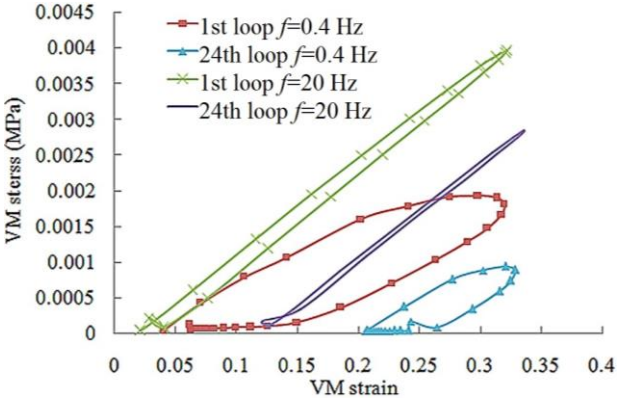

Figure 8. Evolution of a loop between the first cycle and the 24th cycle for f = 0.4 Hz and 20 Hz and μ = 0.2.

3.2.3 Stress relaxation

Stress relaxation curves were obtained for the three adhesion cases by applying a static displacement to the electrode. As shown in Fig. 9, the values for poor adhesion cases are much greater than that for the bonded case. The three curves match perfectly, indicating that the stress relaxation speed is independent of the friction coefficient.

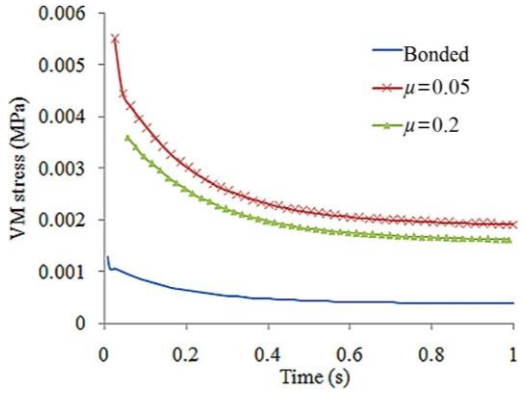

Figure 9. Stress relaxation for the three adhesion cases after application of static displacement.

Based on our results, it is suggested that future neural electrodes should minimize micromotion to the brain tissue. In particular, a biofouling-resistant coating can be used to optimize the interface to enhance the adhesion between the brain tissue and the electrode. In addition, improving the electrode structure, increasing the electrode surface roughness, and using materials with favorable biocompatibility and adhesion as the electrode substrate, such as polymers, can effectively reduce the damage caused by micromotion, and improve the mechanical state of the electrode-brain interface.

4. Conclusion

In this study, a finite element simulation was used for the static and transient analyses of the effects of micromotion frequency and adhesion conditions on the mechanical state of the electrode-brain tissue interface. The results show that the micromotion frequency has a great effect on the maximum VM stress on the finite element model, indicating that higher frequency is more harmful than lower frequency. The critical value is 20 Hz, at which the stress reaches its maximum value, and then increases very slightly with frequency increasing.

The degree of physical coupling between the electrode and brain tissue has a great influence on the interface mechanical state. The results reveal that both the maximum VM stress and VM strain increase with decreasing degree of physical coupling at the electrode-tissue interface. The friction coefficient significantly affects the delamination of brain tissue, with poor adhesion leading to greater delamination than that for good adhesion. A bonded interface leads to lower maximum VM stress and VM strain, and prevents delamination.

The cyclic hysteresis energy is highly dependent on the adhesion of the electrode-tissue interface and the micromotion frequency. The values of VM stress and VM strain are greater for poor adhesion cases, so the cyclic hysteresis energy is greater for the low physical coupling case. For the short-term response, the single-loop area is larger at low frequencies than at high frequencies, but the total hysteresis energy at high frequencies is larger than at low frequencies over a given time period. For the long-term response, the area of a single loop decreases faster for low frequencies than for high frequencies, revealing that the lifetime is shortened under high frequency.

Acknowledgments

The authors gratefully acknowledge the financial support from the National Natural Science Foundation of China (grant 51175334) and the Research Project of State Key Laboratory of Mechanical System and Vibration (grant MSVMS201110).

References

[1] E. Coley, R. Farhadi, S. Lewis and I. R. Whittle, "The incidence of seizures following deep brain stimulating electrode implantation for movement disorders, pain and psychiatric conditions," *Br. J. Neurosurg*., 23: 179-183, 2009.

[2] F. M. Weaver, K. Follett, M. Stern, K. Hur, C. Harris, W. J. Marks Jr, J. Rothlind, O. Sagher, D. Reda and C. S. Moy, "Bilateral deep brain stimulation vs best medical therapy for patients with advanced parkinson disease: a randomized controlled trial," *JAMA-J. Am. Med. Assoc*., 301: 63-73, 2009.

[3] K. E. Lyons and R. Pahwa, "Deep brain stimulation and tremor," *Neurotherapeutics*, 5: 331-338, 2008.

[4] J. Mueller, I. M. Skogseid, R. Benecke, A. Kupsch, T. Trottenberg, W. Poewe, G. H. Schneider, W. Eisner, A. Wolters, J. U. Müller, G. Deuschl, M. O. Pinsker, G. K. Roeste, J. Vollmer-Haase, A. Brentrup, M. Krause, V. Tronnier, A. Schnitzler, J. Voges, G. Nikkhah, J. Vesper, M. Naumann and J. Volkmann, "Pallidal deep brain stimulation improves quality of life in segmental and generalized dystonia: results from a prospective, randomized sham-controlled trial," *Mov. Disord*., 23: 131-134, 2008.

[5] J. D. Simeral, S. P. Kim, M. J. Black, J. P. Donoghue and L. R. Hochberg, "Neural control of cursor trajectory and click by a human with tetraplegia 1000 days after implant of an intracortical microelectrode array," *J. Neural Eng*., 8: 1-24, 2011.

[6] J. P. Seymour and D. R. Kipke, "Neural probe design for reduced tissue encapsulation in CNS," *Biomaterials*, 28: 3594-3607, 2007.

[7] R. Biran, D. C. Martin and P. A. Tresco, "The brain tissue response to implanted silicon microelectrode arrays is increased when the device is tethered to the skull," *J. Biomed. Mater. Res. Part A*, 82: 169-178, 2007.

[8] R. Biran, D. C. Martin and P. A. Tresco, "Neuronal cell loss accompanies the brain tissue response to chronically implanted silicon microelectrode arrays," *Exp. Neurol*., 195: 115-126, 2005.

[9] K. C. Cheung, "Implantable microscale neural interfaces," *Biomed. Microdevices*, 9: 923-938, 2007.

[10] J. P. Seymour and D. R. Kipke, "Neural probe design for reduced tissue encapsulation in CNS," *Biomaterials*, 28: 3594-3607, 2007.

[11] G. C. McConnell, T. M. Schneider, D. J. Owens and R. V. Bellamkonda, "Extraction force and cortical tissue reaction of silicon microelectrode arrays implanted in the rat brain," *IEEE Trans. Biomed. Eng*., 54: 1097-1107, 2007.

[12] A. Gilletti and J. Muthuswamy, "Brain micromotion around implants in the rodent somatosensory cortex," *J. Neural Eng*., 3: 189-195, 2006.

[13] J. Muthuswamy, A. Gilletti, T. Jain and M. Okandan, "Microactuated neural probes to compensate for brain micromotion," *Proc. IEEE Int. Conf. EMBS*, 2: 1941-1943, 2003.

[14] M. Vähäsöyrinki, T. Tuukkanen, H. Sorvoja and M. Pudas, "A minimally invasive displacement sensor for measuring brain micromotion in 3D with nanometer scale resolution," *J. Neurosci. Methods*, 180: 290-295, 2009.
[15] A. K. Lee, J. Epsztein and M. Brecht, "Head-anchored whole-cell recordings in freely moving rats," *Nat. Protoc.*, 4: 385-392, 2009.
[16] H. Lee, R. V. Bellamkonda, W. Sun and M. E. Levenston, "Biomechanical analysis of silicon microelectrode-induced strain in the brain," *J. Neural Eng*., 2: 81-89, 2005.
[17] J. Subbaroyan, D. C. Martin and D. R. Kipke, "A finite-element model of the mechanical effects of implantable microelectrodes in the cerebral cortex," *J. Neural Eng*., 2: 103-113. 2005.
[18] I. Constable, J. G. Williams and D. J. Burns, "Fatigue and cyclic thermal softening of thermoplastics," *J. Mech. Eng. Sci.*, 12: 20-29, 1970.
[19] X. Q. Shi, H. L. J. Pang, W. Zhou and Z. P. Wang, "Low cycle fatigue analysis of temperature and frequency effects ineutectic solder alloy," *Int. J. Fatigue*, 22: 217-228, 2000.
[20] B. Mukherjee and D. J. Burns, "Fatigue-crack growth in polymethylmethacrylate-Effect of frequency, mean and range of stress-intensity factor are covered by the authors in this paper," *Exp. Mech.*, 11: 433-439, 1971.
[21] M. A. Nazari, P. Perrier, M. Chabanas and Y. Payan, "Simulation of dynamic orofacial movements using a constitutive law varying with muscle activation," *Comput. Methods Biomech. Biomed. Eng.*, 13: 469-482, 2010.
[22] M. Hrapko, J. A. Van Dommelen, G. W. Peters and J. S. Wismans, "The influence of test conditions on characterization of the mechanical properties of brain tissue," *J. Biomech. Eng.*, 130: 031003, 2008.
[23] S. Nicolle, M. Lounis, R. Willinger and J. F. Palierne, "Shear linear behavior of brain tissue over a large frequency range," *Biorheology*, 42: 209-223, 2005.
[24] S. S. Margulies and M. T. Prange, "Regional, directional, and age-dependent properties of the brain undergoing large deformation," *J. Biomech. Eng.*, 124: 244-252, 2002.
[25] M. Hrapko, J. A. W. Van Dommelen, G. W. M. Peters and J. Wismans, "The mechanical behaviour of brain tissue: large strain response and constitutive modelling," *Biorheology*, 43: 623-636, 2006.
[26] M. A. Green, L. E. Bilston and R. Sinkus, "In vivo brain viscoelastic properties measured by magnetic resonance elastography," *NMR Biomed.*, 21: 755-764, 2008.